Synthesis, Crystal Structures, Magnetic Properties and Photoconductivity of C_{60} and C_{70} Complexes with Metal Dialkyldithiocarbamates $M(R_2dtc)_x$, where $M = Cu^{II}, Cu^{I}, Ag^{I}, Zn^{II}, Cd^{II}, Hg^{II}, Mn^{II}, Ni^{II}, and Pt^{II}$; R = Me, Et, and nPr

Dmitri V. Konarev,*[a] Andrey Y. Kovalevsky,[b] Salavat S. Khasanov,[c] Gunzi Saito,[d] Dmitri V. Lopatin,[e] Alexey V. Umrikhin,[e] Akihiro Otsuka,[f] and Rimma N. Lyubovskaya[a]

New complexes of fullerenes C_{60} and C_{70} with metal dialkyl-dithiocarbamates, $[M(R_2dtc)_x] \cdot [C_{60(70)}] \cdot [Solvent]$, R = Et [M = Cu^{II} (C_{60}, **1**; C_{70}, **2**), Cu^{I} (C_{60}, **3**; C_{70}, **4**), Ag^{I} (C_{60}, **5**), Zn^{II} (C_{60}, **6**), Cd^{II} (C_{60}, **7**; C_{70}, **8**), Hg^{II} (C_{60}, **9**), Mn^{II} (C_{70}, **10**)], R = Et and Me [M = Cu^{II} (C_{60}, **11**), and Zn^{II} (C_{60}, **12**)], and R = nPr [M = Cu^{II} (C_{60}, **13**), Ni^{II} (C_{60}, **14**), and Pt^{II} (C_{60}, **15**)] were obtained. $M(R_2dtc)_x$ efficiently cocrystallized with fullerene molecules as tetrahedral monomers (**6**, **12**), dimers (**1**, **7**, **11**), and tetramers (**3**, **4**). Fullerene molecules form closely packed hexagonal and square layers in **1**, **7**, and **11**, hexagonal and tetragonal 3D structures in **6** and **12**, and island motifs in **3** and **4**. Complexes **1–15** have a neutral ground state. However, the formation of the complexes with fullerenes changes the environment of paramagnetic Cu^{II} and Mn^{II}. The EPR spectra of **1**, **2**, **11**, and **13** are essentially modified relative to those of pristine $Cu(R_2dtc)_2$ because of a weak coordination of Cu^{II} to fullerene

and a flattening of the central $(NCS_2)_2Cu$ fragments. Complex **10** shows a spectrum exhibiting features from 50 to 600 mT and manifests strong antiferromagnetic coupling of spins with a Weiss temperature of –96 K and the maximum of magnetic susceptibility at 46 K. Such magnetic behavior can be explained by the formation of $[Mn(Et_2dtc)_2]_2$ dimers in **10**. The illumination of the crystals of **1**, **2**, and **7** by white light results in up to a 10^3 increase in photocurrent. The photoconductivity spectra have maxima at 470, 450–650, and 660 nm for **1**, **2**, and **7**, respectively. Photogeneration of free charge carriers is realized by photoexcitation of $Cu(Et_2dtc)_2$ in **1** and **2**, and by charge transfer from $Cd(Et_2dtc)_2$ to C_{60} molecules in **7**. The decrease of photocurrent in **1** and **7** in a weak magnetic field with $B_0 < 0.5$ T was found.

(© Wiley-VCH Verlag GmbH & Co. KGaA, 69451 Weinheim, Germany, 2006)

Introduction

Fullerenes form a wide variety of donor-acceptor complexes ranging from molecular to ionic ones[1–3] with different classes of organic and organometallic donors: aromatic hydrocarbons,[4] amines,[5–7] tetrathiafulvalenes,[6,8] porphyrins and metalloporphyrins,[9–11] porphyrazines,[12] metallocenes,[13–17] and others.[6] Great interest in fullerene complexes was evoked by their intriguing properties. Ionic compounds show ferromagnetism[5] and reversibly form σ-bonded structures.[15–17] Neutral complexes were also used as templates for the preparation of fullerene polymers.[18] They can manifest photoconductivity[19] and excited ionic states upon photoexcitation by white light.[20] The variation of a donor component allows one to affect the packing of fullerene molecules in a crystal, the charged state of fullerenes and, consequently, the properties of the resulting complexes. The search for new classes of donor molecules for the preparation of fullerene complexes can result in the design of new promising compounds. Recently, we have found that dimeric copper(II) diethyldithiocarbamate, $Cu(Et_2dtc)_2$, co-crystallizes with fullerenes to form a molecular complex, $[Cu(Et_2dtc)_2]_2 \cdot C_{60}$, with a layered structure.[21] This work was extended to metal(II) dithiocarbamates with bulkier benzyl substituents (abbreviation: Bnz), namely, $Cu(Bnz_2dtc)_2$, $Ni(Bnz_2dtc)_2$, $Pd(Bnz_2dtc)_2$, and $Pt(Bnz_2dtc)_2$. They co-crystallize with C_{60} to form $M(Bnz_2dtc)_2 \cdot C_{60} \cdot (C_6H_5Cl)_{0.5}$ complexes.[22] In contrast to dimeric $Cu(dedtc)_2$, $M(Bnz_2dtc)_2$ are monomers with planar conformation of the central $(NCS_2)_2M$ fragment, which is charac-

[a] Institute of Problems of Chemical Physics RAS, Chernogolovka, Moscow region 142432, Russia
Fax: +7-96-515-5420
E-mail: konarev@icp.ac.ru
[b] State University of New York at Buffalo, Buffalo, New York, 14260 USA
E-mail: bioayk@langate.gsu.edu
[c] Institute of Solid State Physics RAS, Chernogolovka, Moscow region, 142432, Russia
E-mail: khasanov@issp.ac.ru
[d] Division of Chemistry, Graduate School of Science, Kyoto University,
Sakyo-ku, Kyoto 606-8502, Japan
Fax: +81-75-753-4035
E-mail: saito@kuchem.kyoto-u.ac.jp
[e] Department of Physics, Tambov State University, Tambov, 392622 Russia
E-mail: lopatin@tsu.tmb.ru
[f] Research Center for Low Temperature and Materials Sciences, Kyoto University,
Sakyo-ku, Kyoto, 606-8502, Japan
E-mail: otsuka@kuchem.kyoto-u.ac.jp
Supporting information for this article is available on the WWW under http://www.eurjic.org or from the author.

teristic of Ni^{II}, Pd^{II}, and Pt^{II} dithiocarbamates.[23–27] Moreover, Pd(Bnz$_2$dtc)$_2$ forms a multi-component ionic complex containing C$_{60}$ and bis(benzene)chromium ion-radicals: [Cr^I(C$_6$H$_6$)$_2$$^{·+}$]·(C$_{60}$$^{·–}$)·[Pd(Bnz$_2$dtc)$_2$]$_{0.5}$. The complex demonstrates unusual low-temperature dimerization of C$_{60}$$^{·–}$ with a relatively large hysteresis and the decrease of the dimerization temperature at a fast cooling rate.[22] Thus, metal dialkyldithiocarbamates, M(R$_2$dtc)$_x$, can successfully be used in the design of molecular and ionic complexes with fullerenes. It should be noted that although we have known about M(R$_2$dtc)$_x$ for a long time, their donor-acceptor complexes with π-acceptors are rare. To our knowledge, only some complexes of molybdenum and tungsten dialkyldithiocarbamates with tetracyanoquinodimethane were described.[28,29]

M(R$_2$dtc)$_x$ can easily be modified. It is possible to vary molecular structures of M(R$_2$dtc)$_x$ by changing "M" or the length of alkyl substituents (R). Donor properties of M(R$_2$dtc)$_x$ can also be varied from weak donors to strong ones[30] potentially able to ionize fullerenes. Some of M(R$_2$dtc)$_x$ have broad absorption in the visible range or outstanding magnetic properties [for example, Fe^{III}-(Et$_2$dtc)$_2$Cl is the first single-component ferromagnet with T_c = 2.46 K][31] and, therefore, they can be used as light harvesting or magnetic components for the complexes.

In the present work we studied the effect of M(R$_2$dtc)$_x$ (depending on M and R) on composition, structure, electronic, and physical properties of their complexes with fullerenes. We used monomeric, dimeric, and tetrameric M(R$_2$dtc)$_x$ and varied the length of alkyl (R) substituents (Me, Et, and nPr). M(R$_2$dtc)$_x$ were both weak and strong donors. The interaction of C$_{60}$ with the strongest donors (Cu^I, Mn^{II}, Co^{II}, and V^{II} diethyldithiocarbamates) was studied in benzonitrile solution. Fifteen complexes of C$_{60}$ and C$_{70}$ with Cu^{II}, Cu^I, Ag^I, Zn^{II}, Cd^{II}, Hg^{II}, Mn^{II}, Ni^{II}, and Pt^{II} dialkyldithiocarbamates were obtained and characterized in the solid state. The composition of the complexes was determined from elemental analysis and X-ray diffraction on single crystals. Crystal structures of seven complexes were solved. FTIR- and UV/Visible-NIR spectra of the complexes were studied. Magnetic properties of the complexes with M(R$_2$dtc)$_x$ (M = Cu^I, Cu^{II}, and Mn^{II}) were investigated by SQUID and EPR techniques. Photoconductivity of single crystals of four C$_{60}$ and C$_{70}$ complexes with Cu(Et$_2$dtc)$_2$ and Cd(Et$_2$dtc)$_2$ was studied upon illumination with white light. The comparison of the photoconductivity and the absorption spectra allows one to suggest the mechanisms of free charge carrier generation. The effect of magnetic field with B_0 < 0.5 T on photoconductivity was determined.

Results and Discussion

1. Interaction of Fullerenes with Metal(II) Diethyldithiocarbamates in Solution

The interaction of the strongest M(Et$_2$dtc)$_2$ donors (M = Cu^I, Mn^{II}, Co^{II}, and V^{II}) with C$_{60}$ was studied in solution.

C$_{60}$ and a fivefold molar excess of the corresponding M(Et$_2$dtc)$_x$ were dissolved in benzonitrile at 60 °C over 2 h, the solutions were cooled down, filtered off, and the spectra of the resulting solutions were measured in anaerobic conditions in the 600–1600 nm range. Cu^I, Co^{II}, and V^{II} diethyldithiocarbamates reduce C$_{60}$ to a radical anion, and an absorption band characteristic of C$_{60}$$^-$ is manifested at 1070 nm. On the contrary, Mn(Et$_2$dtc)$_2$ cannot reduce C$_{60}$. These observations are in agreement with redox potentials of metal(II) dithiocarbamates. Related octahedral M^{III}-(dtc)$_3$$^{1–/0}$ (M^{3+}/M^{2+} transition) are reduced at –0.77 V for V$^{3+/2+}$, and –0.92 V for Co$^{3+/2+}$, whereas the reduction potential for Mn$^{3+/2+}$ (–0.08 V) is shifted to positive values (all vs. Ag/AgCl).[30] C$_{60}$ has the first E$^{0/–}$ potential at –0.485 V(vs. Ag/AgCl).[32]

2. Synthesis of Solid Complexes

The complexes obtained and the data from the elemental analysis are listed in Table 1. The ability of M(R$_2$dtc)$_x$ to co-crystallize with C$_{60}$ and C$_{70}$ as well as the composition of the complexes depend on the metal (M) and the length of the alkyl substituents (R). Pristine M(R$_2$dtc)$_2$ (R = Et, nPr) have different conformations of the central (NCS$_2$)$_2$M fragment. Ni(R$_2$dtc)$_2$ and Pt(R$_2$dtc)$_2$ have square planar conformation.[23–27] Zn(R$_2$dtc)$_2$,[33–35] Cd(R$_2$dtc)$_2$,[36,37] and Fe(Et$_2$dtc)$_2$[38] are dimers with a tetrahedral environment of M^{II}. Mn(Et$_2$dtc)$_2$ is a polymer with an octahedral environment of Mn^{II}.[39] Hg(R$_2$dtc)$_2$[40–42] and Cu(R$_2$dtc)$_2$[43] have both square planar or square pyramidal dimeric conformations.

M(Et$_2$dtc)$_2$ (M = Cd^{II}, Hg^{II}, and Mn^{II}) co-crystallize with fullerenes in dimeric conformation to form 1:2 [C$_{60}$/M(R$_2$dtc)$_2$] complexes. As this takes place, Cd(Et$_2$dtc)$_2$, and Mn(Et$_2$dtc)$_2$ precipitate C$_{60}$ and C$_{70}$ complexes from C$_6$H$_6$, C$_6$H$_5$Cl, and C$_6$H$_4$Cl$_2$ solutions in nearly a quantitative yield [a similar ability was found for Fe(Et$_2$dtc)$_2$]. On the contrary, square planar Ni(Et$_2$dtc)$_2$, and Pt(Et$_2$dtc)$_2$ or Co(Et$_2$dtc)$_2$ and V(Et$_2$dtc)$_2$, which reduce C$_{60}$ in solution, do not form crystals of the complexes with fullerenes.

Elongation of alkyl substituents in M(nPr$_2$dtc)$_2$ drastically changes their complex formation with fullerenes. Ni(nPr$_2$dtc)$_2$ and Pt(nPr$_2$dtc)$_2$ with square planar conformation form 2:1 [C$_{60}$/M(nPr$_2$dtc)$_2$] complexes with C$_{60}$. Similarly, among different metal(II) dibenzyldithiocarbamates only Ni(Bnz$_2$dtc)$_2$, Pd(Bnz$_2$dtc)$_2$, and Pt(Bnz$_2$dtc)$_2$ with the same conformation co-crystallize with C$_{60}$.[22] It is interesting to note that Cu(R$_2$dtc)$_2$ form 1:2, 2:1, and 1:1 [C$_{60}$:Cu(R$_2$dtc)$_2$] complexes independently of the R (MeEt, Et, nPr, and Bnz) length. It seems possible that Cu(R$_2$dtc)$_2$ in the complexes with fullerenes can adopt both square planar[43,44] and square pyramidal dimeric conformations.[43]

The crystals of the complexes were obtained by the evaporation of solutions containing fullerenes and corresponding donors. We used the diffusion method to prepare the complexes with air-sensitive M(R$_2$dtc)$_x$ and Cd(Et$_2$dtc)$_2$.

Table 1. Data of elemental analysis for **1**–**15**.

		Elemental analysis found/calcd.						Color and shape
		C [%]	H [%]	N [%]	Cl [%]	S [%]	M [%]	
$[Cu(Et_2dtc)_2]_2 \cdot C_{60}$[a] [21]	**1**	66.46	3.08	4.10	0			black hexagonal
		66.70	2.77	3.88	0	17.77	8.88	plates
$[Cu(Et_2dtc)_2] \cdot (C_{70})_2 \cdot (C_6H_5Cl)_{0.5}$	**2**	83.54	2.24	1.75	0.91			black prisms
		83.51	1.42	1.77	1.12	8.12	4.06	
$\{[Cu^I(Et_2dtc)]_4\}_5 \cdot (C_{60})_3 \cdot (C_6H_4Cl_2)_4$[a]	**3**	51.71	3.11	3.75	5.58			black prisms
		50.75	3.19	4.14	4.21	18.93	18.78	
$\{[Cu^I(Et_2dtc)]_4\}_5 \cdot (C_{70})_3 \cdot (C_6H_4Cl_2)_4$[a]	**4**	53.68	2.97	3.50	4.64			black prisms
		53.26	3.03	3.93	3.93	17.97	17.83	
$Ag^I(Et_2dtc) \cdot C_{60} \cdot C_6H_6$	**5**	82.14	1.48	1.33	–			black prisms
		80.85	1.52	1.32	–	6.07	10.24	
$Zn(Et_2dtc)_2 \cdot C_{60} \cdot (C_6H_5Cl)_{0.5} \cdot (C_6H_6)_{0.5}$[a]	**6**	According to X-ray diffraction data						brown prisms
$\{Cd(Et_2dtc)_2\}_2 \cdot C_{60}$[a]	**7**	61.02	3.04	3.79	–			red-brown rhombus
		61.50	2.67	3.73	–	17.09	15.01	
$\{Cd(Et_2dtc)_2\}_2 \cdot C_{70}$	**8**	64.41	3.32	3.38	<0.7			red-brown rhombus
		65.20	2.41	3.33	0	15.45	13.57	
$\{Hg(Et_2dtc)_2\}_2 \cdot C_{60}$	**9**	56.00	2.35	3.37	–			black hexagonal
		55.02	2.39	3.34	–	15.29	23.96	plates
$\{Mn(Et_2dtc)_2\}_2 \cdot C_{70}$	**10**	68.88[b]	2.59	3.69	0			black elongated parallelepipeds
		70.05	2.98	3.63	0	16.60	7.13	
$[Cu(EtMedtc)_2]_2 \cdot C_{60}$[a]	**11**	66.13	2.21	4.01	–			black rhombus
		65.92	2.31	4.04	–	18.49	9.24	
$[Zn(EtMedtc)_2]_3 \cdot (C_{60})_2$[a]	**12**	According to X-ray diffraction data						black rhombus
$[Cu(nPr_2dtc)_2] \cdot (C_{60})_2$	**13**	86.74	1.48	1.44	0			thin needles
		86.67	1.51	1.51	0	6.89	3.42	
$[Ni(nPr_2dtc)_2] \cdot (C_{60})_2$	**14**	87.01	1.50	1.47	0			thin needles
		86.91	1.50	1.50	0	6.88	3.21	
$[Pt(nPr_2dtc)_2] \cdot (C_{60})_2$	**15**	80.81	2.30	1.70	0			thin needles
		80.93	1.41	1.41	0	6.44	9.81	

[a] The composition of the complex was proved by X-ray diffraction on single crystals. [b] A smaller content of carbon relative to the calculated values may have been caused by the addition of oxygen during elemental analysis because of the high air-sensitivity of $Mn(Et_2dtc)_2$.

3. Crystal Structures

Main geometric parameters of $M(R_2dtc)_x$ and van der Waals (vdW) contacts in the complexes with fullerenes are listed in Table 2. Molecular structures of $M(R_2dtc)_x$ are shown in Figure 1.

The crystal structure of $[Cu(Et_2dtc)_2]_2 \cdot C_{60}$ (**1**) has been described previously.[21]

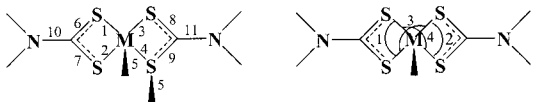$[Cd(Et_2dtc)_2]_2 \cdot C_{60}$ (**7**) has a crystal structure similar to that of **1**. $Cd(Et_2dtc)_2$ and C_{60} molecules are ordered at 120 K. Complex **7** has a layered structure (Figure 2, parts a and b), in which layers of closely packed C_{60} molecules alternate with those composed of $Cd(Et_2dtc)_2$ dimers. Each C_{60} molecule has four neighbors in the layer with the shortest interfullerene center-to-center distance of 9.99 Å along the diagonal to the bc-plane (Figure 2, b). This distance is close to that in pure C_{60} crystals at 153 K (9.94 Å).[45] The vdW C···C contacts are 3.33–3.77 Å. Two other neighboring fullerenes are arranged in the c-direction with a center-to-center distance of 10.54 Å (longer than the vdW diameter of C_{60} molecules of 10.18 Å). Therefore, C_{60} molecules have a square arrangement in the layers.

The projection of the $Cd(Et_2dtc)_2$ layer on the C_{60} one is shown in part b of Figure 2. The central CdS_4 fragments

are arranged strictly above the C_{60} spheres, whereas flexible ethyl substituents occupy available cavities in the C_{60} layers. The effective packing of $Cd(Et_2dtc)_2$ and C_{60} molecules in a crystal is attained due to a butterfly shape of $Cd(Et_2dtc)_2$ dimers (Figure 1), which allows them to encapsulate C_{60} molecules (Figure 2, c).

The packing of $Cd(Et_2dtc)_2$ dimers in the layer has a parquet-like motif (Figure 2, b). The shortest Cd···C(C_{60}) contacts of 3.587 and 3.592 Å are formed with two carbon atoms of the 6–6 bond of C_{60}. These contacts are noticeably longer than the Cu···C(C_{60}) contacts in **1** (3.334 and 3.379 Å).[21] Co-crystallization of $Cd(Et_2dtc)_2$ with C_{60} does not affect its geometry. The pristine donor has a dimeric structure with a nearly tetrahedral environment of Cd^{II} with three short equatorial bonds and one short axial bond (an average length is 2.575 Å). One equatorial bond is noticeably longer than the other ones (2.812 Å).[36] The dimeric structure of $Cd(Et_2dtc)_2$ is retained in **7**. Averaged lengths of three short equatorial bonds and one short axial bond are nearly the same (2.577 Å), but the long equatorial bond is elongated to 2.877 Å. Two of four ethyl groups of $Cd(Et_2dtc)_2$ are directed towards the fullerene layer in **7** (Figure 2, c), whereas in **1** three of four ethyl groups of $Cu(Et_2dtc)_2$ are directed towards the fullerene layer.[21]

Table 2. Geometric parameters for metal dialkyldithiocarbamates in the complexes with fullerenes.

Complex Geometry	1 Dimer	11 Dimer	7 Dimer	3 Tetramer[a]	4 Tetramer[a]	6 Tetrahedral monomer	12 Tetrahedral monomer[b]
Bond lengths [Å]							
1	2.3354(8)	2.3057(15)	2.8771(10)	2.245(3)–	2.247(3)–	2.3449(9)	2.340(3)
2	2.2978(9)	2.3361(12)	2.544(9)	2.281(3)	2.278(3)	2.3390(9)	2.343(3)
3	2.2994(9)	2.3389(12)	2.5333(10)			2.3425(10)	2.394(3)
4	2.3218(8)	2.3177(14)	2.6330(10)			2.3350(9)	2.357(3)
5	3.030(1)	2.7869(12)	2.5988(12)			–	–
6	1.725 (3)	1.718(5)	1.758(4)			1.705(4)	1.695(13)
7	1.722(3)	1.707(5)	1.714(3)	1.700(10)–	1.698(11)–	1.735(3)	1.712(14)
8	1.720(3)	1.717(6)	1.737(3)	1.764(10)	1.777(10)	1.733(3)	1.743(12)
9	1.724(3)	1.724(5)	1.717(4)			1.733(6)	1.1.754(11)
10	1.321(4)	1.328(7)	1.337(4)	1.324(4)–	1.317(14)–	1.340(5)	1.281(14)
11	1.320(4)	1.335(7)	1.331(5)	1.335(4)	1.342(15)	1.326(4)	1.355(16)
M···S (**1–4**) aver.	2.3135	2.3246	2.6468	2.2567	2.2618	2.3403	2.358
Bond angles [°]							
1	76.90(3)	76.73(5)	66.67(3)	122.6(1)–	121.83(11)–	77.89(3)	78.17(12)
2	77.06(3)	76.44(5)	70.29(3)	123.18(11)	123.65(10)	78.29(3)	78.15(13)
3	164.84(3)	162.67(6)	143.80(3)			127.18(4)	129.21(13)
4	173.00(3)	169.49(5)	157.64(4)			128.19(4)	130.28(12)
M···M distances [Å]	3.529(1)	3.561(2)	3.802(2)	tetrahedron 2.5855(17)– 2.6239(17)	tetrahedron 2.5698(18)– 2.6306(18)	–	–
Donor–Fullerene interactions, shortest vdW contacts							
M···C(Ful.) [Å]	3.269, 3.307	3.334, 3.379	3.587, 3.592	4.800, 4.838	4.437,4.476	3.659, 3.822	3.66–3.94
S···C(Ful.) [Å]	3.52–3.89	3.52–3.95	3.51–3.80	3.59–3.99	3.66–3.84	3.35–3.76	3.43–3.63
N···C(Ful.) [Å]	3.68–3.81	3.72–3.77	3.52–3.77	3.89–3.95	3.66–3.95	3.37–3.52	3.65–3.75
H···C(Ful.) [Å]	2.84–2.94	2.97–3.00	2.86–3.13	2.92–3.26	2.78–3.08	2.95–3.13	3.06–3.28
Fullerene–Fullerene interaction							
Packing of fullerenes	hexagonal layers, 6 neighbors	hexagonal layers, 6 neighbors	square layers, 4 neighbors	isolated	isolated	hexagonal, 3D, 6 neighbors	tetragonal, 3D, 4 neighbors
Interfullerene center-to-center distances [Å]	10.02 (×4), 10.25 (×2)	9.89 (×4), 10.02 (×2)	9.99 (×4)	shortest 13.5	shortest 13.5	10.38 (×2), 10.13, 9.93, 9.81, 9.74	9.83, 9.86, 9.88, 10.09
Interfullerene C···C contacts [Å]	3.329–3.466, –	3.276–3.410, 3.392–3.470	3.328–3.770, –	–	–	3.250–3.360	3.269–3.410

[a] The ranges for the bond lengths and angles are given for **3** and **4**. [b] The bond lengths and angles for Zn(EtMedtc)$_2$ are given for one of three crystallographically independent molecules.

[Cu(EtMedtc)$_2$]$_2$·C$_{60}$ (**11**) is isostructural to **1**. The substitution of two of four ethyl groups by methyl ones results in the decrease of the unit cell parameters of **11** relative to those of **1** (see Table 4). C$_{60}$ and Cu(EtMedtc)$_2$ molecules are ordered. Complex **11** also has a layered structure (Figure 3, a and b) with six neighbors to each C$_{60}$ molecule. The shortest interfullerene center-to-center distances are 9.89 (four neighbors along the diagonal to the *bc*-plane) and 10.02 Å (two neighbors in the *c*-direction; Figure 3, b). For both cases the vdW C···C contacts between adjacent fullerenes of 3.28–3.41 and 3.39–3.47 Å are shorter than 3.42 Å and center-to-center distances are close to the dis-

tance in pure C$_{60}$[45] justifying the formation of closely packed hexagonal layers.

The projection of the Cu(EtMedtc)$_2$ layer on the C$_{60}$ layer is shown in Figure 3, b. The central CuS$_4$ fragments arranged above C$_{60}$ spheres allow two flexible ethyl groups to occupy cavities in the C$_{60}$ layers. C$_{60}$ forms shortened Cu···C(C$_{60}$) contacts of 3.334 and 3.379 Å by two carbon atoms of one 6–6 bond (Figure 3, b). VdW S, N and H···C(C$_{60}$) contacts are close to those in **1** and **7** (Table 2).

Cu(EtMedtc)$_2$ has a dimeric structure in **11** with a square pyramidal environment of Cu^{II} atoms (Figure 1) with four
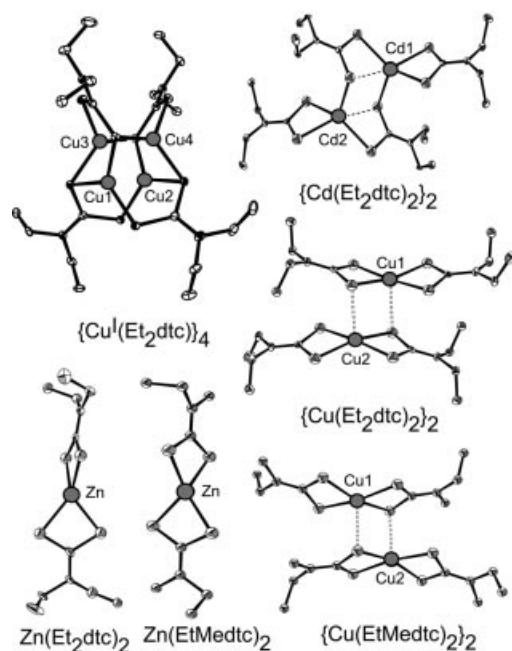
Figure 1. Molecular structures of $M(R_2dtc)_x$ in the complexes with fullerenes: $\{Cd(Et_2dtc)_2\}_2$, $\{Cu(Et_2dtc)_2\}_2$ and $\{Cu(EtMedtc)_2\}_2$ dimers; tetrahedral $Zn(Et_2dtc)_2$ and $Zn(EtMedtc)_2$ monomers and $[Cu^I(Et_2dtc)]_4$ tetramers.

short equatorial bonds (the average length is 2.325 Å) and one relatively long axial bond (2.787 Å). Both ethyl groups of $Cu(EtMedtc)_2$ are directed towards the fullerene layer.

Thus, **1**, **7**, and **11** have similar crystal structures. However, the differences in the molecular structures of $M(R_2dtc)_2$ and the length of the alkyl substituents provide their noticeable modifications. The packing motif of the fullerene layer changes from closely packed hexagonal layers in **11**, to intermediate layers in **1** (four and two neighbors with 10.02 and 10.25 Å center-to-center interfullerene distances)[21] and finally to square layers in **7**. The character of $M(R_2dtc)_2$-fullerene interactions also changes. Weakly bound $Cu(R_2dtc)_2$ dimers with relatively long axial bonds have a more planar shape of the $(NCS_2)_2M$ fragments than those in strongly bound $Cd(Et_2dtc)_2$ dimers with a short axial bond. The dihedral angles between the NCS_2M planes are 160.9 and 158.6° in **1** and **11**, and only 143.8° in **7** providing shorter $Cu\cdots C(C_{60})$ distances (by about 0.3 Å) in **11** and **1** than the $Cd\cdots C(C_{60})$ distances in **7**. However, the more concave surface of the $Cd(Et_2dtc)_2$ fragments results in better conditions for the π-π interaction between the NCS_2Cd planes and two adjacent C_{60} hexagons (Figure 2, c) since the dihedral angle of 143.8° is close to that between adjacent C_{60} hexagons (138.5°). As a result, the NCS_2Cd planes and the C_{60} hexagons arrange parallel to each other with the dihedral angles between them equal only to 0.8 and 8.2°. High steric complementarity is probably a reason for the ability of $Cd(Et_2dtc)_2$ to quantitatively precipitate C_{60} and C_{70} complexes from solutions. More planar $Cu(R_2dtc)_2$ provides worse conditions for the π-π interac-
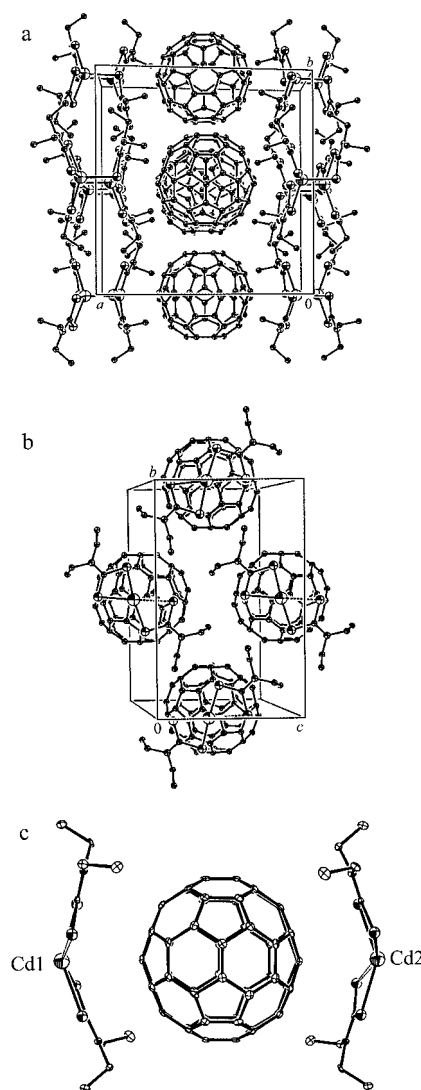

Figure 2. Crystal structure of **7**: the view of the unit cell on the *ab*-(a) and *bc*-planes (b); a mutual arrangement of concave Cd-$(Et_2dtc)_2$ fragments and a spherical C_{60} molecule (c).

tions in **1** and **11** with corresponding dihedral angles of 9.8, 13.6° and 9.5, 12.6°, respectively.

$Zn(Et_2dtc)_2 \cdot C_{60} \cdot (C_6H_5Cl)_{0.5} \cdot (C_6H_6)_{0.5}$ (**6**) crystallizes in a triclinic lattice. C_{60} and $Zn(Et_2dtc)_2$ molecules are ordered, whereas C_6H_5Cl and C_6H_6 molecules share one position with equal occupancies and are disordered. Complex **6** has a unique cage structure with large channels along the *a*-axis accommodating $Zn(Et_2dtc)_2$ and solvent molecules. The channels are completely surrounded by the fullerene molecules, which form a hexagonal 3D framework (Figure 4). Each C_{60} molecule has six neighbors. The center-to-center distances for three of them (9.74, 9.81, and 9.93 Å) are close to that distance in pure C_{60},[45] whereas the other ones are larger (10.38 Å ×2 and 10.13 Å). Shortened vdW $C\cdots C$ contacts between the closest fullerenes are 3.250–3.360 Å.

$Zn(Et_2dtc)_2$ forms a complex with C_{60} in a monomeric state with nonplanar *pseudo*-tetrahedral configuration of Zn^{II} (the dihedral angle between two NCS_2Zn planes being
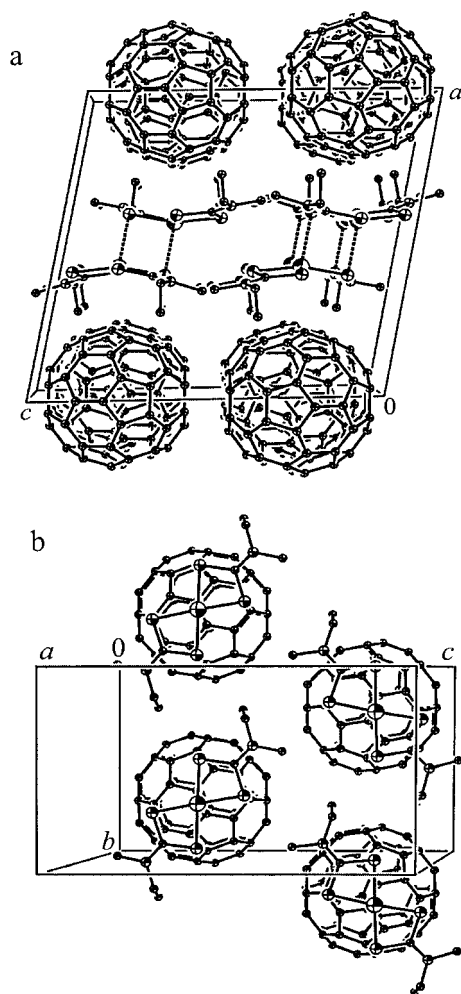
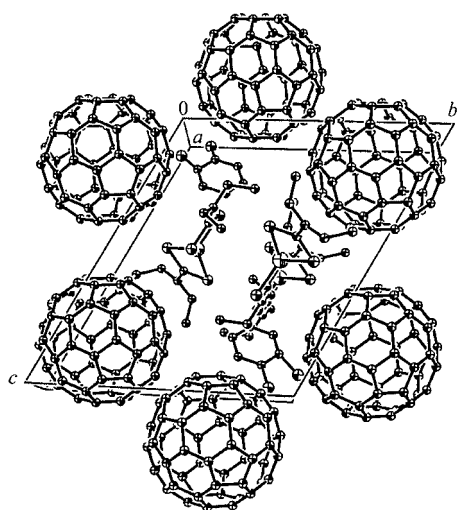Figure 3. Crystal structure of **11**: the view of the unit cell of **11** on the *ac*- (a) and *bc*-planes (b).

91.5°) (Figure 1). This conformation is for the first time observed for Zn(Et$_2$dtc)$_2$. Similar geometry of the (NCS)$_2$Zn fragment was reported for Zn(Bnz$_2$dtc)$_2$ with bulky benzyl substituents,[46] whereas pristine Zn(R$_2$dtc)$_2$ with R = Et, *n*Pr, *i*Pr substituents have dimeric structures.[33–35]

Because of the tetrahedral geometry, only half of each Zn(Et$_2$dtc)$_2$ molecule forms vdW contacts with C$_{60}$ (Table 2). The closest Zn···C(C$_{60}$) distances are 3.659 and 3.822 Å. The other half of the Zn(Et$_2$dtc)$_2$ molecule locates above the adjacent Zn(Et$_2$dtc)$_2$.

The substitution of two ethyl groups by methyl ones changes the packing motif in [Zn(EtMedtc)$_2$]$_3$·(C$_{60}$)$_2$ (**12**). In contrast to previously described complexes, both C$_{60}$ molecules are disordered at 90 K between two orientations with 66/34 and 58/42% occupancies. These orientations are linked by the rotation of the C$_{60}$ molecule by 180° about the axis passing through the centers of two oppositely located 5–6 bonds. There is also certain disorder in the positions of ethyl and methyl groups in Zn(EtMedtc)$_2$. The complex has 3D packing of fullerenes, in which each C$_{60}$ molecule has four neighbors and is located in the center of a distorted tetrahedron. This 3D packing can be split in strongly puckered C$_{60}$ layers parallel to the *ac*-plane (Figure 5). Three neighbors are seen in this plane, whereas the fourth neighbor is located in the adjacent layers. The center-to-center distances are in the 9.83–10.09 Å range (the vdW radius of C$_{60}$ is 10.18 Å) and the shortest C···C contacts lie in the 3.27–3.41 Å range. The cavities in the 3D framework are occupied by Zn(EtMedtc)$_2$ molecules. One Zn-(EtMedtc)$_2$ molecule arranges parallel to the *ac*-plane and two other ones are perpendicular to this plane (Figure 5). Because of the strong puckering of fullerene layers, each Zn(EtMedtc)$_2$ molecule forms vdW contacts with four fullerene ones. The Zn···C(C$_{60}$) distances of 3.66–3.94 Å are similar to those in **6**.

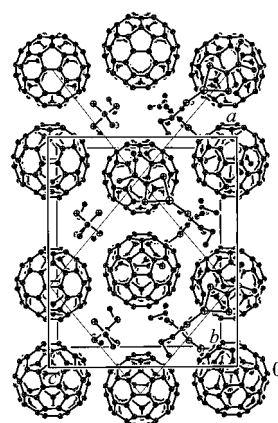Figure 4. The view of the unit cell of **6** along the *a*-axis.

Figure 5. The view of the crystal structure of **12** on the *ac*-plane. C$_{60}$ molecules occupy two levels. Molecules belonging to one level are connected by thin lines.

{[Cu^I(Et$_2$dtc)]$_4$}$_5$·(C$_{60}$)$_3$·(C$_6$H$_4$Cl$_2$)$_4$ (**3**) and {[Cu^I-(Et$_2$dtc)]$_4$}$_5$·(C$_{70}$)$_3$·(C$_6$H$_4$Cl$_2$)$_4$ (**4**) are isostructural and have high-symmetry cubic unit cells with parameters of

43.7822(4) (**3**) and 44.2911(3) (**4**) Å and unusually great volumes of 83925.3(13) (**3**) and 86885.9(10) Å (**4**). Two symmetrically independent C_{60} molecules are disordered. One of them is located on a twofold axis and the other molecule is on a fourfold axis. Because of the disorder, C_{60} molecules have two and four orientations, respectively. $[Cu^{I}(Et_2dtc)]_4$ and solvent $C_6H_4Cl_2$ molecules are located in general positions and are ordered.

The complexes have an island motif of fullerene packing with the shortest interfullerene center-to-center distances of 13.5 Å. Loose layers can be outlined in the *bc*-plane. The main structural motif of these layers is shown in Figure 6. There are large (right in Figure 6) and small (left in Figure 6) squares consisting of five and four fullerene molecules. Each small square is surrounded by four large squares and vice versa. As this takes place, both squares have one common C_{60} molecule. Small squares accommodate five $[Cu^{I}(Et_2dtc)]_4$ molecules, whereas large squares accommodate eight $[Cu^{I}(Et_2dtc)]_4$ and eight $C_6H_4Cl_2$ molecules. It is interesting that all eight $C_6H_4Cl_2$ molecules surround one C_{60} molecule (Figure 6). The adjacent fullerene layers in 3D packing are arranged in such a way that large fullerene squares are located above and below small fullerene squares.
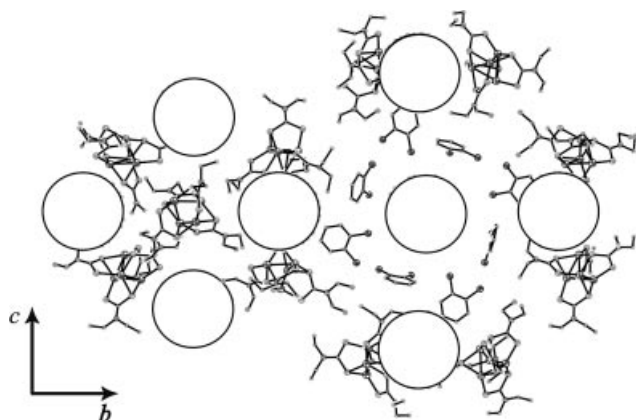

Figure 6. The view of the crystal structure of **3** on the *bc*-plane.

$[Cu^{I}(Et_2dtc)]_4$ is a tetramer containing four $Cu^{I}(Et_2dtc)$ units (Figure 1). Cu^{I} atoms form a slightly distorted tetrahedron with the Cu···Cu distance of 2.5698(18)–2.6306(18) Å. Each Cu^{I} atom forms three Cu–S coordination bonds of 2.245(3)–2.281(3) Å length. Therefore, the coordination number of Cu^{I} is 3. Pristine $Cu^{I}(Et_2dtc)$ and $Au^{I}(Et_2dtc)$ form dimers,[47,48] and for $Ag^{I}(Et_2dtc)$ hexamers and polymers are also known.[49,50] According to the best of our knowledge, a tetrameric structure is for the first time observed for $Cu^{I}(Et_2dtc)$. Probably, the formation of complexes with C_{60} and C_{70} stabilizes the tetrameric structure. The Cu···$C(C_{60})$ and Cu···$C(C_{70})$ distances (4.80 and 4.44 Å), as well as the vdW N and S···C(fullerene) contacts (Table 2) are large enough to show low efficiency of the π-π interaction in **3** and **4**.

4. Magnetic Properties of the Complexes

EPR spectroscopy is a sensitive tool used to study changes in a local environment of Cu^{II} atoms at the formation of fullerene complexes with $Cu(R_2dtc)_2$. Pristine $Cu(R_2dtc)_2$ with R = Et, nPr possess dimeric structures with square pyramidal geometry of Cu^{II} (the coordination number is 5).[43] Such geometry is characterized by the EPR spectrum shown in part a of Figure 7. $Cu(EtMedtc)_2$ has an asymmetric structure and as a result shows a more asymmetric EPR signal (Supporting Information).
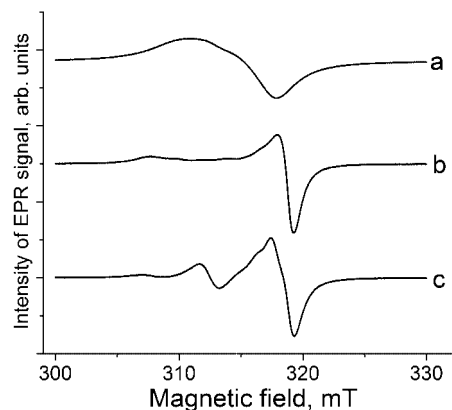

Figure 7. The EPR spectra of polycrystalline pristine $Cu(Et_2dtc)_2$ (a); **1** (b), and **2** (c) at 290 K.

The EPR signal of **1** (Figure 7, b) is noticeably different from that of pristine $Cu(Et_2dtc)_2$. According to X-ray diffraction data, $Cu(Et_2dtc)_2$ has a dimeric structure in **1** as well.[21] However, noticeable changes are observed in the environment of Cu^{II}. Weak axial coordination of Cu^{II} to C_{60} with a rather short Cu···$C(C_{60})$ distance of 3.27 Å enhances the asymmetry of the environment of Cu^{II}. This coordination directs oppositely to the axial Cu–S bond and results in noticeable elongation of this bond from 2.844(1) in the pristine donor to 3.030(2) Å in **1**. Consequently, the central $(NCS_2)_2Cu$ fragments become more planar in **1** than in the pristine donor. Coordination of Cu^{II} to C_{60} is more favorable for planar conformation of $M(Et_2dtc)_2$, and most probably namely this coordination evokes the flattening of the central $(NCS_2)_2Cu$ fragments. The M···$C(C_{60})$ distances (3.587, 3.334, and 3.269 Å) decrease together with the flattening of $M(Et_2dtc)_2$ fragments in the following order: **7**, **11**, and **1** (the length of axial M–S bonds are 2.599, 2.787, and 3.030 Å, respectively).

The EPR spectra of $[Cu(Et_2dtc)_2]·(C_{70})_2·(C_6H_5Cl)_{0.5}$ (**2**, Figure 7, c), $[Cu(EtMedtc)_2]_2·C_{60}$ (**11**), and $[Cu(nPr_2dtc)_2]·$ $(C_{60})_2$ (**13**) (for spectra of **11** and **13** see supporting information) are also noticeably changed relative to those of pristine $Cu(R_2dtc)_2$. These changes are similar to those observed in the spectrum of **1** suggesting that weak coordination of Cu^{II} to fullerenes and a flattening of the central $(NCS_2)_2Cu$ fragments can be realized in these complexes as well.

D. V. Konarev et al.

Magnetic susceptibilities of **1** and **2** were measured from 300 down to 1.9 K and were shown to follow the Curie–Weiss law with the small negative Weiss constants of –2.5 K (**1**) and –2.0 K (**2**), which indicate only a weak antiferromagnetic interaction between Cu^{II} centers. Axial Cu–S bonds transfer the magnetic interaction in the {Cu-(Et₂dtc)₂}₂ dimers and their elongation at the formation of complexes with fullerenes can weaken the antiferromagnetic interaction between Cu^{II} centers.

The spectrum of C_{60} and an excess of $Cu^I(Et_2dtc)$ in benzonitrile shows that CT is realized from donor to fullerene molecules in solution. To study CT in the solid state we measured the EPR spectra (4–290 K) and magnetic susceptibilities of {[$Cu^I(Et_2dtc)]_4$}₅·(C_{60})₃·($C_6H_4Cl_2$)₄ (**3**) and {[$Cu^I(Et_2dtc)]_4$}₅·(C_{70})₃·($C_6H_4Cl_2$)₄ (**4**) in the 2–300 K range. Pristine $Cu^I(Et_2dtc)$ is diamagnetic and EPR silent. **3** and **4** are also diamagnetic with temperature-independent diamagnetic contributions of –0.00522 and –0.00666 emu/mol⁻¹. Paramagnetic contributions of the Curie impurities are only 0.23 and 1.3% for **3** and **4**. According to EPR at 290 K (two narrow lines with $g_1 = 2.0009$ and $g_2 = 2.0025$ for **3** and one narrow line with $g = 2.0019$ for **4**) these impurities originate mainly from defects.[51] Thus, in spite of the observation of CT in solution, both complexes are molecular ones in the solid state. Most probably, this is associated with the formation of [$Cu^I(Et_2dtc)]_4$ tetramers, whose shape is unfavorable for effective CT to fullerene molecules.

It is known that pristine $Mn^{II}(Et_2dtc)_2$ has a polymeric structure with a distorted octahedral environment of Mn^{II}.[39] In EPR it shows a single Lorentzian line with $g = 2.0115$ and $\Delta H = 61.8$ mT (Figure 8, a), which is characteristic of this environment of Mn^{II}.[52] The formation of {$Mn(Et_2dtc)_2$}₂·C_{70} (**10**) results in considerable changes in the EPR spectrum indicating noticeable modification of the local environment of Mn^{II}. The EPR spectrum exhibits features extending from 50 to about 500 mT (Figure 8, b). Such a spectrum is typical for dinuclear Mn^{II} species[53] and previously a very similar EPR spectrum has been observed, for example, in a dinuclear Mn^{II} complex bridged by chlorine atoms.[54] Magnetic susceptibility data provides evidence of a strong exchange interaction between Mn^{II} cen-
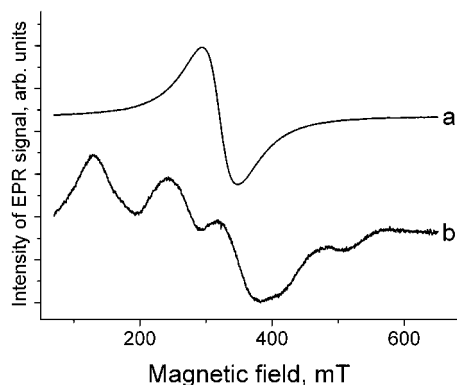

Figure 8. The EPR spectra of polycrystalline pristine $Mn(Et_2dtc)_2$ (a) and polycrystalline **10** (b) at 290 K.

ters. The magnetic moment of **10** is equal to 7.78 μ$_B$ per formula unit at 300 K, which is close to the calculated value of 7.75 μ$_B$ if two 5/2 spins contribute to magnetic susceptibility. Mn^{II} spins interact antiferromagnetically in the 150–300 K range with a large negative Weiss constant of –96 K and magnetic susceptibility decreases below 46 K (Figure 9). Such exchange interactions between Mn^{II} can be realized if $Mn(Et_2dtc)_2$ forms dimers in **10** [similar to {$Cd(Et_2dtc)_2$}₂ dimers in **7**]. EPR data support this conclusion. The EPR signal from $Mn(Et_2dtc)_2$ in **10** remains unchanged qualitatively down to 4 K. No EPR signals attributed to C_{70}·⁻ [55] were found indicating the absence of CT to fullerene molecules. Thus, $Mn(Et_2dtc)_2$ cannot ionize C_{70} in the solid state. Similarly, $Mn^{II}TPP$ (tetraphenylporphyrinate) ($E^{+/0}_{1/2} = -0.23$ V vs. SCE)[56] forms only molecular complexes with fullerenes C_{60} and C_{70}.[57]
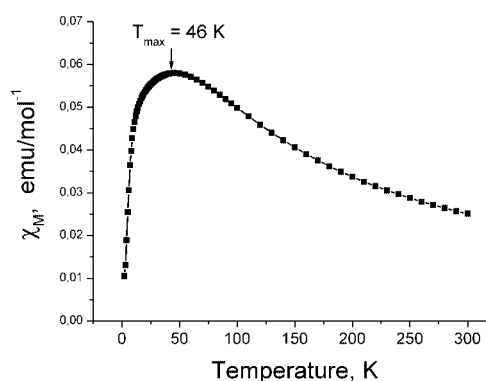

Figure 9. Molar magnetic susceptibility of polycrystalline **10** in the 1.9–300 K range.

5. IR- and UV/Visible-NIR Spectra of the Complexes

The IR spectra of **1–15** (see Supporting Information) are a superposition of those of pristine metal dithiocarbamates, fullerenes, and solvent molecules. The positions of peaks in the UV/Visible-NIR spectra of **1–15** and pristine donors are listed in Table 3. The absence of absorption in the NIR spectra of **1–15** at 1070 nm indicates neutral ground states of the complexes. Pristine $Cu(Et_2dtc)_2$ has broad absorption in the visible range with the maximum at 442 nm and a shoulder at 660 nm (Figure 10, part 1, c). This absorption retains in the spectra of the complexes with the maximum at 437 nm (**1**, Figure 10, part 1, b) and 455 nm (**2**, Figure 10, part 1, a). The bands at 341 and 263 nm (**1**) and 230 nm (**2**) were ascribed to intramolecular transitions in fullerenes.[58] The spectra of **6** (Figure 10, part 2, b) and **7** (Figure 10, part 2, a) also contain C_{60} absorption bands at 263 and 340 nm and a relatively weak band at 470 nm. The latter band ascribed to intermolecular CT between neighboring C_{60} molecules was also found in the spectra of fullerene films.[59] A condition necessary for the observation of this band in the solid-state spectra of the complexes is close packing of fullerene molecules in the crystal.[7,60] Since C_{60} molecules are closely packed in **1**, **7**, and **6**, this band can manifest itself in their spectra. However, in the spectrum

Table 3. UV/Vis-NIR spectra of the starting compounds and **1**–**15**.

Compounds	The bands of fullerenes [nm]	M[d(alkyl)dtc]$_x$ [nm]	CT bands [nm] **A** (Full.)	**C** (D.-Full.)
C_{60}	262 s, 341 s		470 m	
C_{70}	–, 420 s, 540 m			
Cu(EtMedtc)$_2$		267 s, 438 s, ca. 660 w		
Cu(Et$_2$dtc)$_2$		271 s, 442s, ca. 660 w		
Cu(nPr$_2$dtc)$_2$		277 s, 449s, ca. 650 w		
Ni(nPr$_2$dtc)$_2$		322 s, 389 s, 606 w		
1	263 s[a], 341 s	263 s[a], 434 m[a], ca. 650 w		–
2	383 s, 455 m[a]	455 m[a]		
3	262 s, 340 m			
4	383 s, 480 m			
5	263 s, 334 s			
6	261 s, 337 s			
7	263 s, 340 s		470 w	610 w
8	379 s, 462 m			
9	255 s, 332 s			
10	388 s, 484 m			
11	265 s[a], 337 s	265 s[a], 443 m[a], ca. 650 w		–
12	261 s, 338 m			
13	262 s[a], 341 s	262 s[a], 434 m,[a] ca. 615 w	434 m[a]	900 w
14	266 s, 340 s,	ca. 605 w[a]	450 w	ca. 770 w[a]
15	266 s, 340 s		450 w	650 w

[a] The bands overlap.

of **1** it is closed by absorption of Cu(Et$_2$dtc)$_2$. A similar interfullerene CT band was reported for pristine C_{70} at 550 nm,[59] and it can also contribute to broad absorption of **2** at 500–600 nm (Figure 10, part 1, a).

The spectrum of **7** additionally contains a broad weak band at 610 nm (Figure 10, part 2, a). Because C_{60} and Cd(Et$_2$dtc)$_2$ do not absorb noticeably in this range, it can be attributed to intermolecular CT from Cd(Et$_2$dtc)$_2$ to C_{60}. The observation of this band is possible due to favorable π-π interaction between Cd(Et$_2$dtc)$_2$ and C_{60} molecules (Figure 2, c). CT bands are absent in the spectra of **6** (Figure 10, part 2, b) and **1**–**5**, **8**–**12** (Supporting Information) indicating worse conditions for the π-π interaction between nonplanar M^{II}(R$_2$dtc)$_x$ and fullerenes. Absorption at 600–700 nm in the spectra of **1**, **2**, and **11** was attributed mainly to Cu(R$_2$dtc)$_2$ (a shoulder at 660 nm).

Several processes can occur at photoexcitation of **1**, **2**, and **7** in the visible range. In **1** and **2** mainly photoexcitation of Cu^{II}(Et$_2$dtc)$_2$ (437 and 660 nm) is realized together with a minor contribution of intermolecular CT between neighboring C_{60} and C_{70} molecules (470 and 550 nm, respectively), whereas in **7** intermolecular CT from Cd(Et$_2$dtc)$_2$ to C_{60} molecules (610 nm) and between C_{60} molecules (470 nm) is mainly realized.

The absorption spectra of **13** and pristine Cu(nPr$_2$dtc)$_2$ are shown in part 3 of Figure 10. Additionally to absorption of Cu(nPr$_2$dtc)$_2$ in the visible range (Figure 10, part 3, a, and Table 3), the intense band with the maximum at 900 nm (Figure 10, part 3, a) was attributed to CT from the Cu(nPr$_2$dtc)$_2$ to the C_{60} molecules. Similar bands are observed in the spectra of **14** and **15**. Therefore, planar M(nPr$_2$dtc)$_2$ have better conditions for the π-π interaction with fullerenes than nonplanar M[(Et, Me)$_2$dtc]$_2$.

6. Photoconductivity in C_{60} and C_{70} Complexes with Cu(Et$_2$dtc)$_2$ and Cd(Et$_2$dtc)$_2$ (**1**, **2**, **7**, and **8**)

According to the IR- and EPR data, **1**, **2**, **7**, and **8** are molecular complexes without CT in the ground state. The crystals of **1**, **2**, and **7** have low "dark" conductivity $\sigma \approx 10^{-10}$ to 10^{-11} S·cm^{-1}. The photoexcitation of single crystals of the complexes by white light from a 150 W halogen tube with 10^{12} to 10^{14} photons/cm^2·s intensity results in a 20–50-fold increase in the photocurrent in **1**, two orders of magnitude in **2**, and three orders of magnitude in **7**. These values remain unchanged under the illumination of the crystals for 10^4 s and are completely reproducible. The crystals of **8** do not show a noticeable increase in photocurrent at photoexcitation.

Photoconductivity spectra of the complexes are shown in Figure 11. Photoconductivity has maxima at 470 nm for **1**, 450–650 nm for **2**, and about 660 nm for **7**. The comparison of the photoconductivity spectra of **1**, **2**, and **7** with their absorption spectra allows one to suppose the mechanisms of free charge carrier generation. In **1** and **2** the main contribution is given by the photoexcitation of Cu(Et$_2$dtc)$_2$ (440 and 660 nm) as well as interfullerene CT between neighboring C_{60} or C_{70} molecules (470 nm for **1** and 550 nm for **2**, Figure 11, a and b). The major contribution is given in **7** by CT from the Cd(Et$_2$dtc)$_2$ to the C_{60} molecule (610 nm) with a small contribution of interfullerene CT between neighboring C_{60} molecules (470 nm) (Figure 11, c). In spite of similar crystal structures, the mechanisms of free charge carrier generation are different in **1** and **7**. In **1** Cu(Et$_2$dtc)$_2$ has intense absorption in the visible range, whereas Cd(Et$_2$dtc)$_2$ is transparent in **7** in this range. However, steric compatibility of the Cd(Et$_2$dtc)$_2$ and C_{60} molecules (Figure 2, c) provides better
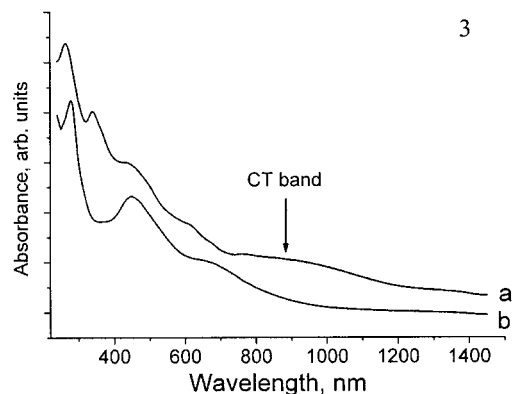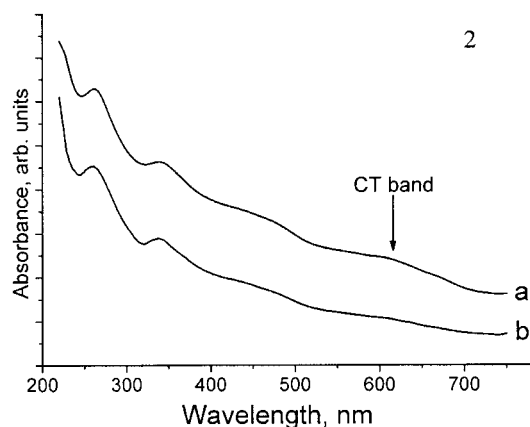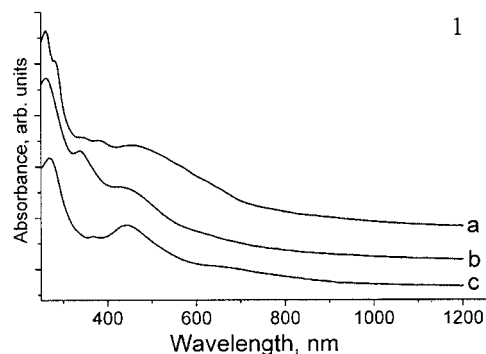
Figure 10. The UV/Visible-NIR spectra of: (1) **2** (a); **1** (b); and pristine $Cu(Et_2dtc)_2$ (c). (2) **7** (a); and **6** (b). (3) **13** (a); and pristine $Cu(nPr_2dtc)_2$ (b) in KBr pellets.
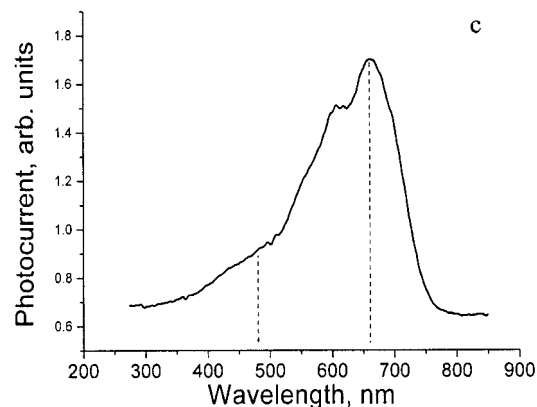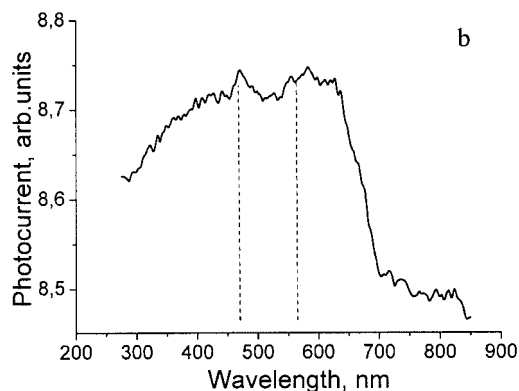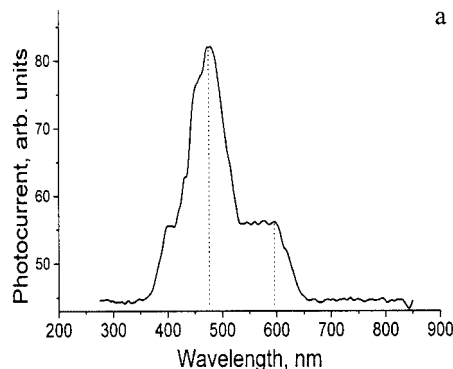
Figure 11. Photoconductivity spectra of the crystals of **1** (a), **2** (b), and **7** (c). The positions of the main peaks in the spectra are shown by dashed lines.

conditions for the π-π interaction and correspondingly for intermolecular CT in **7** than in **1**. Complex **8** has no CT band in the visible range and as a result photoconductivity was not found in this complex.

Photoconductivity of **1** and **7** is sensitive to weak magnetic field (MF) with $B_0 < 0.5$ T (Figure 12). A negative MF effect on photoconductivity is because of the reaction involving triplet CT excitons and paramagnetic centers. This interaction releases charges from deep-seated traps and increases photocurrent. A collision of triplet CT-excitons

with doublet paramagnetic species may lead either to spin-independent triplet scattering or quenching. During quenching a transition from the initial spin state, which is a mixture of a doublet and a quartet, to a purely doublet final state takes place:

$$^3T + {}^2R \underset{k_{-1}}{\overset{k_1}{\rightleftarrows}} {}^{2,4}(^3T...^2R) \overset{k_L}{\longrightarrow} {}^1S + {}^2R$$
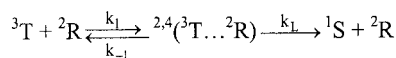
The rate constant k_L of the transition from each of the six L-th initial spin states of an intermediate complex to a final one depends on the amplitude of the doublet compo-

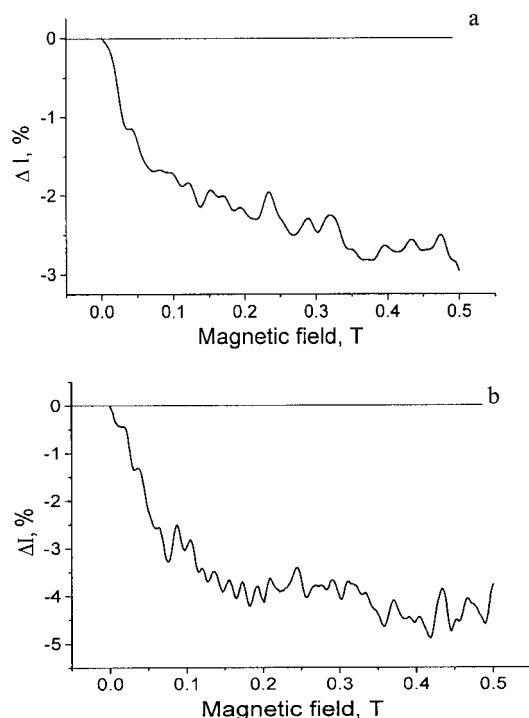Figure 12. Magnetic field (B_0, T) dependence of photocurrent (I, %) in **1** (a) and **7** (b).

nent therein. The total rate of exciton quenching by paramagnetic impurity is:

$$Q = \frac{1}{6} k_1 \sum_{L=1}^{6} \frac{k_L}{k_{-1} - k_L} ,$$

where k_1 and k_{-1} are rate constants of collision and back scattering, respectively. The value of Q has a maximum, when a doublet component is uniformly distributed over all six substates, the minimum of Q is attained at the complete separation of a doublet and a quartet. The quenching rate is maximal in ZMF. With the application of an external MF, the doublet component concentrates on four states and the value of Q decreases together with the rate of dissociation of CT excitons and, consequently, a number of free charge carriers. A similar negative MF dependence was found in anthracene.[61]

Conclusions

We studied the formation of the complexes between metal dialkyldithiocarbamates, $M(R_2dtc)_x$ with R = EtMe (Cu^{II}, Zn^{II}); Et (Cu^{II}, Cu^{I}, Ag^{I}, Zn^{II}, Cd^{II}, Hg^{II}, Mn^{II}, Fe^{II}, Co^{II}, V^{II}, Ni^{II}, and Pt^{II}); nPr (Cu^{II}, Cu^{I}, Zn^{II}, Cd^{II}, Ni^{II}, and Pt^{II}) and fullerenes C_{60} and C_{70}. It was shown that $M(R_2dtc)_x$ co-crystallize with fullerenes C_{60} and C_{70} to form complexes of different structures and compositions (**1–15**). Pristine $M(R_2dtc)_x$ (R = Et, nPr) have a large variety of molecular structures in fullerene complexes, which can be square planar or tetrahedral monomers, strongly and weakly bound dimers and tetramers. Tetrahedral mo-

nomeric conformations for $Zn(EtMedtc)_2$ and $Zn(Et_2dtc)_2$ and tetrameric $\{Cu^{I}(Et_2dtc)\}_4$ were for the first time found for these metal dithiocarbamates.

Butterfly-shaped $[M\{(Me, Et)_2dtc\}_2]_2$ dimers (M = Cu and Cd) form layered structures in **1**, **7**, and **11**, where the packing of C_{60} layers varies from a square to hexagonal one. The dimeric structure of dithiocarbamates provides a characteristic 1:2 composition of the complexes {Fullerene/$M[(Et, Me)dtc]_2$}. Complexes **8**–**10** have the same composition, and $M(R_2dtc)_2$ can have similar dimeric structures in these complexes. This supposition was justified for **10** by magnetic data. $Cd(Et_2dtc)_2$ has geometry conforming well to the spherical shape of fullerene molecules and shows high ability to nearly quantitatively precipitate C_{60} and C_{70} complexes from solutions. A similar ability was found for $Mn(Et_2dtc)_2$ and $Fe(Et_2dtc)_2$. Monomeric $Ni(nPr_2dtc)_2$ and $Pt(nPr_2dtc)_2$ with square planar conformation of the central $(NCS_2)_2M$ fragment form **12** and **13** with a 2:1 composition [Fullerene/$M(nPr_2dtc)_2$]. Complexes **2** and **13** have the same composition and the formation of $Cu(Et_2dtc)_2$ and $Cu(nPr_2dtc)_2$ monomers can be supposed for these complexes as well especially because pristine $Cu(R_2dtc)_2$ can adopt a square planar conformation.[43,44] However, X-ray diffraction data are needed to prove this supposition. Non-planar tetrahedral $Zn(EtMedtc)_2$ and $Zn(Et_2dtc)_2$ provide 3D packing of fullerenes with their tetrahedral and hexahedral arrangements. Bulky $[Cu^{I}(Et_2dtc)]_4$ promotes an island motif in fullerene packing.

Using $M(Et_2dtc)_x$ with different donor ability (the strongest donors contain M = Cu^{I}, Co^{II}, V^{II}, and Mn^{II}) we found that $Cu^{I}(R_2dtc)$, $Co(R_2dtc)_2$, and $V(R_2dtc)_2$ reduce C_{60} in benzonitrile. However, among these strong donors only fullerene complexes with $Mn(Et_2dtc)_2$ and $Cu^{I}(Et_2dtc)$ were obtained as crystals and no CT to fullerene molecules was found in them. The EPR spectra of paramagnetic $Cu(R_2dtc)_2$ and $Mn(Et_2dtc)_2$ noticeably change at the complex formation with fullerenes most probably due to changes in the environment of M^{II}. The EPR spectra of **1**, **2**, **11**, and **13** are noticeably modified relative to those of pristine $Cu(R_2dtc)_2$. Such changes can be a result of additional weak coordination of Cu^{II} to C_{60} and the flattening of the central $(NCS_2)_2Cu$ fragment. The changes in the EPR spectrum of $Mn(Et_2dtc)_2$ at the formation of **10** are most probably evoked by the transition from a polymeric structure of pristine $Mn(Et_2dtc)_2$ with an octahedral environment of Mn^{II} to the formation in **10** of $\{Mn(Et_2dtc)_2\}_2$ dimers, in which strong antiferromagnetic exchange interaction between Mn^{II} centers is possible.

The spectra of the complexes in the visible and NIR ranges indicate their neutral ground state. $Cu(R_2dtc)_2$ (**1**, **2**, **11**, and **13**) and $Ni(nPr_2dtc)_2$ (**14**) absorb in the visible range, whereas other $M(R_2dtc)_2$ are nearly transparent in this range. In addition to the bands associated with intramolecular transitions in fullerenes and $M(R_2dtc)_x$, the bands associated with intermolecular CT between neighboring fullerene molecules (at 470 nm for C_{60} and at 550 nm for C_{70})[59] and CT from $M(R_2dtc)_2$ to fullerene molecules are observed. The latter CT bands are observed only in the

spectra of **7** and the complexes with planar $M(nPr_2dtc)_2$ (**13–15**). The other complexes demonstrate either weak or no CT bands indicating worse conditions for the π-π interaction between fullerenes and nonplanar $M(R_2dtc)_x$. In accordance with the neutral ground state, the crystals of **1**, **2**, and **7** show low dark conductivity of 10^{-10} to 10^{-11} S·cm^{-1}. The illumination of the crystals by white light with 10^{12} to 10^{14} photons/cm^2·s intensity results in up to a 10^3 increase in photocurrent. The photoconductivity spectra exhibit maxima at 470, 450–650, and 660 nm for **1**, **2**, and **7**, respectively. Three processes generate free charge carriers in the complexes. Photoexcitation of $Cu(Et_2dtc)_2$ contributes to photoconductivity of **1** and **2** since this donor has intense absorption in the visible range. A similar mechanism was observed in $Bz_4BTPE\cdot C_{60}$ {Bz$_4$BTPE: tetrabenzo[1,2-bis(4*H*-thiopyran-4-ylidene)ethane]},[62] and conjugated polymer-fullerene composites.[63] CT from donor to fullerene molecules contributes to photoconductivity of the complexes with relatively intense CT bands in the visible-NIR range: **7** and TBPDA·(C$_{60}$)$_2$ (N,N,N',N'-tetrabenzyl-p-phenylenediamine).[19] Interfullerene CT between neighboring fullerene molecules also contributes to photoconductivity in **1** and **7** as well as in pure fullerene crystals[64] and films.[59] Common peculiarity of the C$_{60}$ complexes showing photoconductivity is a layered arrangement of fullerene and donor molecules in a crystal, which allow the movement of photogenerated carriers through the crystal. Weak MF with $B_0 < 0.5$ T differently affects photoconductivity of fullerene complexes. We found negative (**1** and **7**) and positive $(Bz_4BTPE\cdot C_{60})$[64] MF dependences as well as the field dependence with sign inversion at 0.3 T [TBPDA·(C$_{60}$)$_2$].[19] A variety of dependences indicates that the interaction of MF with photogenerated excitons can be different in fullerene complexes depending on the donor used. The mechanisms of the effects of MF on photoconductivity involve triplet CT excitons and paramagnetic centers[61] or the population of a triplet state from a singlet one in MF.[65] Thus, fullerene complexes with M{Et$_2$dtc}$_2$ and other M{R$_2$dtc}$_x$ may be a new wide family of photoactive compounds. A study of the photophysical properties of these complexes is now in progress.

Experimental Section

Materials: Sodium diethyldithiocarbamate trihydrate, [Na(Et$_2$dtc)·3H$_2$O], was purchased from Aldrich and recrystallized from an acetonitrile/benzene mixture. Sodium ethylmethyldithiocarbamate, Na(EtMedtc), and sodium di(n-propyl)dithiocarbamate, Na(nPr$_2$dtc), were obtained by the reported procedure.[43] Carbon disulfide (3.1 mL, 0.052 mol) and sodium hydroxide (50% aqueous solution, 4 mL) were added to a stirred solution of R$_2$NH (0.05 mol) (R$_2$NH=EtMeNH, Aldrich, and nPr$_2$NH, Wako) in ethanol (5 mL) at $T < 4$ °C (ice bath). After stirring for 4–6 h at $T < 4$ °C Na(EtMedtc) precipitated as white crystals. Na(nPr$_2$dtc) was obtained by the evaporation of an ethanol/water solution without heating. Pure Na(R$_2$dtc) were obtained by recrystallization from acetonitrile/benzene mixtures (50–80% yields). Air-sensitive M(R$_2$dtc)$_x$ compounds (R = Et, M = Cu^I, Co^{II}, V^{II}, Fe^{II}, and Mn^{II}; R = nPr, M = Cu^I) were obtained by stirring anhydrous CuCl

(100 mg), CoBr$_2$ (150 mg), VCl$_2$ (100 mg), FeBr$_2$ (150 mg), and MnI$_2$ (150 mg) and x [x = 1 (Cu^I) or 2 (other metals)] molar equivalents of Na(Et$_2$dtc) in 10 mL of degassed acetonitrile over 4 h in a glove box. M(R$_2$dtc)$_x$ were precipitated from acetonitrile as light yellow (Cu^I and Mn^{II}), light pink (Fe^{II}), dark green-brown (Co^{II}), and light brown (V^{II}) powders together with NaCl(Br, I). The precipitates were washed with acetonitrile (3 mL) and dried. NaCl(Br, I) as well as possible admixtures of unreacted MCl(Br, I)$_x$ and Na(Et$_2$dtc) were separated from M(R$_2$dtc)$_x$ at a stage of complex formation with fullerene because of their insolubility in *o*-dichlorobenzene (C$_6$H$_4$Cl$_2$). Air-stable M(R$_2$dtc)$_2$ (R = EtMe, M = Cu^{II}, and Zn^{II}; R = Et, M = Cu^{II}, Zn^{II}, Cd^{II}, Hg^{II}, Ag^I, Ni^{II}, and Pt^{II}; R = nPr, M = Cu^{II}, Zn^{II}, Cd^{II}, Ni^{II}, and Pt^{II}) were obtained in aqueous solution from CuBr$_2$, ZnCl$_2$, CdBr$_2$·4H$_2$O, Hg(NO$_3$)$_2$·H$_2$O, AgNO$_3$, NiCl$_2$, PtCl$_2$, and Na(R$_2$dtc).[43] M(R$_2$dtc)$_2$ were dissolved in hot chlorobenzene (C$_6$H$_5$Cl), filtered off from NaCl, NaBr, or NaNO$_3$ and the solvent was removed to dryness on a rotary evaporator to yield pure M(R$_2$dtc)$_2$ with satisfactory elemental analyses (50–80% yield). C$_{60}$ of 99.98% purity and C$_{70}$ of 99.0% purity were used from MTR Ltd. Solvents were purified under argon. C$_6$H$_4$Cl$_2$ and C$_6$H$_5$Cl were distilled over CaH$_2$. Hexane and benzonitrile (C$_6$H$_5$CN) were distilled over Na/benzophenone. For the synthesis of air-sensitive M(R$_2$dtc)$_x$ (R = Et, M = Cu^I, Co^{II}, V^{II}, Fe^{II}, and Mn^{II}; R = nPr, M = Cu^I) and the preparation of the fullerene complexes, solvents were degassed and stored in a MBraun 150B-G glove box with a controlled atmosphere with contents of H$_2$O and O$_2$ of less than 1 ppm. The crystals of **3**, **4**, and **10** were stored in a glove box and were sealed in 2-mm quartz tubes for EPR and SQUID measurements under 10^{-5} Torr. KBr pellets for IR- and UV/Visible-NIR measurements were prepared in a glove box.

Synthesis: The composition of **1–5**, **7–11**, and **13–15** was determined from the elemental analysis (Table 1) and was justified for **1**, **3**, **4**, **6**, **7**, **11**, and **12** by X-ray diffraction on a single crystal.

The crystals of **1**, **2**, **5**, **6**, **9**, and **11–15** were obtained by a slow evaporation of chlorobenzene solution (15 mL) containing C$_{60}$ (25 mg, 0.0347 mmol) and two molar equivalents of M(R$_2$dtc)$_x$ (0.06940 mmol) over 1 week. The crystals precipitated were washed with an excess of acetone (50–80% yield). The shapes of the crystals are presented in Table 1.

The crystals of **3** and **4** were obtained under anaerobic conditions by a slow diffusion of hexane (20 mL) in C$_6$H$_4$Cl$_2$ solution (20 mL) containing C$_{60}$ (25 mg, 0.0347 mmol) (**3**) or C$_{70}$ (20 mg, 0.0238 mmol) (**4**) and a fourfold molar excess of Cu^I(Et$_2$dtc) in a glass tube of 45 mL volume with a ground glass plug. After 1 month large black prisms of **3** and **4** were precipitated on the wall of the tube (up to $0.5 \times 0.5 \times 0.8$ mm^3 size). The solvent was decanted and the crystals were washed with hexane (50–60% yield).

Cd(Et$_2$dtc)$_2$, Mn(Et$_2$dtc)$_2$, and Fe(Et$_2$dtc)$_2$ nearly quantitatively precipitate C$_{60}$ and C$_{70}$ from different solvents (C$_6$H$_6$, C$_6$H$_5$Cl, and C$_6$H$_4$Cl$_2$). Because of this, the crystals of **7** and **8** were obtained by the diffusion of a benzene solution (20 mL) of C$_{60}$ (20 mg, 0.02775 mmol) (**7**) or C$_{70}$ (20 mg, 0.0238 mmol) (**8**) in CHCl$_3$ solution (20 mL) containing a twofold molar excess of Cd(Et$_2$dtc)$_2$. The crystals precipitated on the wall of the tube after 1 month. They were washed with acetone (70–90% yield).

The crystals of **10** were obtained similarly under anaerobic conditions by the diffusion of benzene solution (20 mL) of C$_{70}$ (20 mg, 0.0238 mmol) (**8**) into C$_6$H$_4$Cl$_2$ containing a twofold molar excess of Mn(Et$_2$dtc)$_2$. The crystals precipitated on the wall of the tube after 1 month. They were washed with hexane (70% yield).

Table 4. X-ray diffraction data for **1**, **3**, **4**, **6**, **7**, **11**, and **12**.

	1[21]	**3**	**4**
Structural formula	$[Cu(Et_2dtc)_2]_2 \cdot C_{60}$	$\{[Cu^I(Et_2dtc)]_4\}_5 \cdot (C_{60})_3 \cdot (C_6H_4Cl_2)_4$	$\{[Cu^I(Et_2dtc)]_4\}_5 \cdot (C_{70})_3 \cdot (C_6H_4Cl_2)_4$
Empirical formula	$C_{80}H_{40}Cu_2N_4S_8$	$C_{76}H_{54}Cl_2Cu_5N_5S_{10}$	$C_{83.50}H_{54}Cl_2Cu_5N_5S_{10}$
M_r [g·mol^{-1}]	1440.72	1746.41	1836.52
Crystal shape and color	black hexagonal prisms	black cubes	black cubes
Size [mm×mm×mm]	$0.40 \times 0.30 \times 0.25$	$0.50 \times 0.40 \times 0.40$	$0.40 \times 0.30 \times 0.30$
Crystal system	monoclinic	cubic	cubic
Space group	$P2_1/c$	$Pn\bar{3}n$	$Pn\bar{3}n$
a [Å]	16.1948(8)	43.7822(4)	44.2911(3)
b [Å]	10.2552(5)	43.7822(4)	44.2911(3)
c [Å]	17.2192(9)	43.7822(4)	44.2911(3)
α [°]	90	90	90
β [°]	102.504(2)	90	90
γ [°]	90	90	90
V [Å^3]	2791.9(2)	83925.3(13)	86885.9(10)
Z	2	48	48
ρ_{calc} [g/cm^3]	1.714	1.655	1.685
μ [mm^{-1}]	1.12	1.921	1.860
$F(000)$	1468	42240	44592
Absorption correction	no correction	no correction	SADABS[66]
Max./min. transmission	0.77/0.66	0.51/0.45	0.60/0.52
T [K]	90(2)	90(2)	90(1)
Max. 2θ [°]	54.12	50.04	50.04
Reflections measured	25977	524031	690665
Unique reflections	5683	12379	12798
R_{int}	0.036	0.0429	0.0637
Parameters, restraints	425, 0	450, 0	458, 0
Reflections [$F_o > 2\sigma(F_o)$]	4983	9398	8774
R_1 [$F_o > 2\sigma(F_o)$]	0.0404	0.0984	0.0935
wR_2 (all data)[a]	0.1064	0.2904	0.3181
a	0.0341	0.1060	0.1330
b	8.2311	2219.48	2964.08
G.O.F.	1.082	1.132	1.054
Restr. G.O.F.	1.082	1.132	1.054
CCDC number	260289	286142	286143

	6	**7**	**11**	**12**
Structural formula	$Zn(Et_2dtc)_2 \cdot C_{60} \cdot (C_6H_5Cl)_{0.5} \cdot (C_6H_6)_{0.5}$	$[Cd(Et_2dtc)_2]_2 \cdot C_{60}$	$[Cu(EtMedtc)_2]_2 \cdot C_{60}$	$[Zn(EtMedtc)_2]_3 \cdot (C_{60})_2$
Empirical formula	$C_{76}H_{25.5}Cl_{0.5}N_2S_4Zn$	$C_{80}H_{40}Cd_2N_4S_8$	$C_{76}H_{32}Cu_2N_4S_8$	$C_{144}H_{54}N_6S_{12}Zn_3$
M_r [g·mol^{-1}]	1177.82	1538.44	1384.62	2442.71
Crystal shape and color	black parallelepipeds	brown rhombus	black rhombus	black rhombus
Size [mm×mm×mm]	$0.33 \times 0.20 \times 0.20$	$0.40 \times 0.30 \times 0.10$	$0.42 \times 0.38 \times 0.10$	$0.40 \times 0.30 \times 0.20$
Crystal system	triclinic	monoclinic	monoclinic	orthorhombic
Space group	$P\bar{1}$	$P2_1/c$	$P2_1$	$Pn2_1a$
a [Å]	10.3762(5)	16.1712(13)	16.0626(4)	20.815(5)
b [Å]	15.1717(7)	16.9680(12)	10.0196(3)	26.072(6)
c [Å]	17.0002(8)	10.5355(8)	17.0653(5)	17.128(4)
α [°]	115.893(1)	90	90	90
β [°]	91.555(1)	99.857(2)	100.9490(13)	90
γ [°]	102.938(1)	90	90	90
V [Å^3]	2322.53(19)	2848.2(4)	2696.51(13)	9298.88(12)
Z	2	2	2	4
ρ_{calc} [g/cm^3]	1.684	1.794	1.705	1.746
μ [mm^{-1}]	0.797	1.098	1.156	1.109
$F(000)$	1196	1544	1404	4944
Absorption correction	SADABS[66]	SADABS[66]	no correction	no correction
Max./min. transmission	0.86/0.78	0.90/0.72	0.89/0.64	0.81/0.66
T [K]	90(1)	123(2)	100(2)	100(2)
Max. 2θ [°]	58.0	51.88	54.96	51.48
Reflections measured	25011	13023	20222	42780
Unique reflections	7276	3602	11660	17592
R_{int}	0.03	0.0333		
Parameters, restraints	724, 10	424, 423	812, 0	2393, 11252
Reflections [$F_o > 2\sigma(F_o)$]	6312	3100	10282	8450
R_1 [$F_o > 2\sigma(F_o)$]	0.042	0.0358	0.0381	0.1038
wR_2 (all data)[a]	0.1177	0.085	0.0902	0.3023
a	0.0582	0.040	0.0294	0.1956
b	5.0135	5.096	3.4011	0.0000
G.O.F.	1.042	1.055	1.033	0.954
Restr. G.O.F.	1.056	1.006	1.033	0.758
CCDC number	286144	288291	288292	288293

[a] (a) $w = 1/[\sigma^2(F_o^2) + (aP)^2 + bP]$, $P = [\max(F_o^2, 0) + 2 F_c^2]/3$.

The C_{60} complexes with $Mn(Et_2dtc)_2$ and $Fe(Et_2dtc)_2$ were also obtained as powders by mixing C_{60} (25 mg, 0.0347 mmol) and a twofold molar excess of $M(Et_2dtc)_2$ in $C_6H_4Cl_2$ (20 mL) on heating (60 °C, 2 h). The hot solution was filtered, cooled down to room temperature, and stood overnight. The solution became colorless, and a light brown polycrystalline precipitate was formed. However, in contrast to crystals of **10**, powdered samples did not show reasonable elemental analyses probably because of the high air-sensitivity of the complexes. Indeed, $Mn(Et_2dtc)_2$ and $Fe(Et_2dtc)_2$ are extremely air-sensitive and oxidize in a few seconds in air.

We tried to crystallize the C_{60} complexes with $Co(Et_2dtc)_2$ and $V(Et_2dtc)_2$. C_{60} (25 mg, 0.0347 mmol) and a twofold molar excess of $M(Et_2dtc)_2$ were dissolved in $C_6H_4Cl_2$ (20 mL) on stirring at 60 °C for 4 h. The hot solution was filtered, cooled down to room temperature, and filtered in a glass tube of 45 mL volume with a ground glass plug. Slow diffusion of hexane (20 mL) was carried out under anaerobic conditions. However, only black powder without crystals formed after 2 months.

General: UV/Visible-NIR spectra were measured with a Shimadzu-3100 spectrometer in the 240–2600 nm range. FT-IR spectra were measured in KBr pellets with a Perkin–Elmer 1000 Series spectrometer (400–7800 cm^{-1}). A Quantum Design MPMS-XL SQUID magnetometer was used to measure static magnetic susceptibilities of **1**–**4** and **10** from 1.9 up to 300 K. A sample holder contribution and core temperature independent diamagnetic susceptibility (χ_0) were subtracted from the experimental values. The values of Θ, χ_0 were calculated using the appropriate formula: $\chi_M = C/(T - \Theta) + \chi_0$. EPR spectra were recorded for **1**, **2**, **11**, and **13** at room temp. and for **3**, **4**, and **10** from RT down to 4 K with a JEOL JES-TE 200 X-band ESR spectrometer equipped with a JEOL ES-CT470 cryostat. Photoconductivity of **1**, **2**, **7**, and **8** was excited using a white light halogen tube with 10^{12}–10^{14} photons/cm^{2}s intensity. To record the spectra of photoconductivity the light beam of a xenon lamp was transmitted through a high-aperture monochromator. A static magnetic field with the induction up to 1 T was generated by an electromagnet of a Radiopan SE/X 2547 ESR spectrometer.

X-ray Crystal Structure Determination: X-ray diffraction data for **1**, **3**, **4**, **6**, **7**, **11**, and **12** were collected with a Bruker SMART1000 CCD diffractometer installed at a rotating anode source (Mo-K$_a$ radiation, $\lambda = 0.71073$ Å), and equipped with an Oxford Cryosystems nitrogen gas-flow apparatus. The data were collected by the rotation method with 0.3° frame-width (ω scan) and 10 s exposure time per frame. Four sets of data (600 frames in each set) were collected, nominally covering half of the reciprocal space. The data were integrated, scaled, sorted and averaged using the SMART software package.[66] The structures were solved by the direct methods using SHELXTL NT Version 5.10.[67] The structure was refined by full-matrix least-squares against F^2. The details of the X-ray crystal structure analysis for **1**, **3**, **4**, **6**, **7**, **11**, and **12** including CCDC numbers for the structures are given in Table 4. Non-hydrogen atoms were refined in the anisotropic approximation. Positions of hydrogen atoms were calculated geometrically. Subsequently, the positions of H-atoms were refined by the "riding" model with $U_{iso} = 1.2U_{eq}$ of the connected non-hydrogen atom or as ideal CH_3 groups with $U_{iso} = 1.5U_{eq}$. The supplementary crystallographic data for this paper can be obtained free of charge from The Cambridge Crystallographic Data Centre via www.ccdc.cam.ac.uk/data_request/cif.

Supporting Information (for details see the footnote on the first page of this article): IR-data, UV/Vis-NIR spectra of pristine donors and complexes **1**–**15**, and EPR spectra of pristine Cu-

$(EtMedtc)_2$ and $Cu(nPr_2dtc)_2$ and complexes **11** and **13** (Tables S1 and S2, Figures S1–S7).

[1] A. L. Balch, M. M. Olmstead, *Chem. Rev.* **1998**, *98*, 2123–2165.
[2] D. V. Konarev, R. N. Lyubovskaya, *Russ. Chem. Rev.* **1999**, *68*, 19–38.
[3] C. A. Reed, R. D. Bolskar, *Chem. Rev.* **2000**, *100*, 1075–1120.
[4] A. L. Litvinov, D. V. Konarev, A. Y. Kovalevsky, I. S. Neretin, Y. L. Slovokhotov, P. Coppens, R. N. Lyubovskaya, *CrystEngComm* **2002**, *4*, 618–622.
[5] P.-M. Allemand, K. C. Khemani, A. Koch, F. Wudl, K. Holczer, S. Donovan, G. Grüner, J. D. Thompson, *Science* **1991**, *253*, 301–303.
[6] D. V. Konarev, R. N. Lyubovskaya, N. V. Drichko, E. I. Yudanova, Y. M. Shul'ga, A. L. Litvinov, V. N. Semkin, B. P. Tarasov, *J. Mater. Chem.* **2000**, *10*, 803–818.
[7] D. V. Konarev, A. Y. Kovalevsky, A. L. Litvinov, N. V. Drichko, B. P. Tarasov, P. Coppens, R. N. Lyubovskaya, *J. Solid State Chem.* **2002**, *168*, 474–485.
[8] G. Saito, T. Teramoto, A. Otsuka, Y. Sugita, T. Ban, M. Kusunoki, K. Sakaguchi, *Synth. Met.* **1994**, *64*, 359–368.
[9] M. M. Olmstead, D. A. Costa, K. Maitra, B. C. Noll, S. L. Phillips, P. M. Van Calcar, A. L. Balch, *J. Am. Chem. Soc.* **1999**, *121*, 7090–7097.
[10] P. D. W. Boyd, M. C. Hodgson, C. E. F. Rickard, A. G. Oliver, L. Chaker, P. J. Brothers, R. D. Bolskar, F. S. Tham, C. A. Reed, *J. Am. Chem. Soc.* **1999**, *121*, 10487–10495.
[11] D. V. Konarev, I. S. Neretin, Y. L. Slovokhotov, E. I. Yudanova, N. V. Drichko, Y. M. Shul'ga, B. P. Tarasov, L. L. Gumanov, A. S. Batsanov, J. A. K. Howard, R. N. Lyubovskaya, *Chem. Eur. J.* **2001**, *7*, 2605–2616.
[12] D. H. Hochmuth, S. L. J. Michel, A. J. P. White, D. J. Williams, A. G. M. Barrett, B. M. Hoffman, *Eur. J. Inorg. Chem.* **2000**, 593–596.
[13] J. D. Crane, P. B. Hitchcock, H. W. Kroto, R. Taylor, D. R. M. Walton, *J. Chem. Soc. Chem. Commun.* **1992**, 1764–1765.
[14] W. C. Wan, X. Liu, G. M. Sweeney, W. E. Broderick, *J. Am. Chem. Soc.* **1995**, *117*, 9580–9581.
[15] A. Hönnerscheid, L. van Wüllen, M. Jansen, J. Rahmer, M. Mehring, *J. Chem. Phys.* **2001**, *115*, 7161–7165.
[16] D. V. Konarev, S. S. Khasanov, A. Otsuka, G. Saito, *J. Am. Chem. Soc.* **2002**, *124*, 8520–8521.
[17] D. V. Konarev, S. S. Khasanov, G. Saito, A. Otsuka, Y. Yoshida, R. N. Lyubovskaya, *J. Am. Chem. Soc.* **2003**, *125*, 10074–10083.
[18] D. Y. Sun, C. A. Reed, *Chem. Commun.* **2000**, 2391–2392.
[19] D. V. Lopatin, V. V. Rodaev, A. V. Umrikhin, D. V. Konarev, A. L. Litvinov, R. N. Lyubovskaya, *J. Mater. Chem.* **2005**, *15*, 657–660.
[20] D. V. Konarev, G. Zerza, M. C. Scharber, N. S. Sariciftci, R. N. Lyubovskaya, *Mol. Crys. Liq. Crys.* **2005**, *427*, 315–333.
[21] D. V. Konarev, A. Y. Kovalevsky, D. V. Lopatin, V. V. Rodaev, A. V. Umrikhin, E. I. Yudanova, P. Coppens, R. N. Lyubovskaya, G. Saito, *Dalton Trans.* **2005**, 1821–1825.
[22] D. V. Konarev, A. Y. Kovalevsky, A. Otsuka, G. Saito, R. N. Lyubovskaya, *Inorg. Chem.* **2005**, *44*, 9547–9556.
[23] A. Bonamiko, G. Dessy, C. Mariani, A. Vaciago, L. Zambonelli, *Acta Crystallogr.* **1965**, *19*, 619–626.

[24] A. Z. Amanov, G. A. Kukina, M. A. Porai-Koshits, *Dokl. Akad. Nauk Az. SSR* **1977**, *33*, 23–26.

[25] J. Lokaj, V. Vrabel, E. Kello, *Chem. Zvesti* **1984**, *38*, 313–317.

[26] M.-L. Riekkola, T. Pakkanen, L. Niinisto, *Acta Chem. Scand. Ser. A* **1983**, *37*, 807–812.

[27] P. W. G. Newnan, A. H. White, *J. Chem. Soc. Dalton Trans.* **1972**, 2239–2243.

[28] M. Decoster, F. Conan, J. E. Guerchais, Y. Le Mest, J. Sala Pala, J. C. Jeffery, E. Faulques, A. Leblanc, P. Molinié, *Polyhedron* **1995**, *14*, 1741–1750.

[29] F. Conan, J. Sala Pala, M.-T. Garland, R. Baggio, *Inorg. Chim. Acta* **1998**, *278*, 108–112.

[30] H. L. M. Van Gaal, J. G. M. Van der Linden, *Coord. Chem. Rev.* **1982**, *47*, 41–54.

[31] H. H. Wickman, A. M. Trozzolo, H. J. Williams, G. W. Hull, F. R. Merritt, *Phys. Rev.* **1967**, *155*, 563–566.

[32] D. Dubois, K. M. Kadish, S. Flanagan, R. E. Haufler, L. P. F. Chibante, L. J. Wilson, *J. Am. Chem. Soc.* **1991**, *113*, 4364–4366.

[33] M. Bonamico, G. Mazzone, A. Vaciago, L. Zambonelli, *Acta Crystallogr.* **1965**, *19*, 898–909.

[34] N. Sreehari, B. Varghese, P. T. Manoharan, *Inorg. Chem.* **1990**, *29*, 4011–4015.

[35] H. Miyamae, M. Ito, H. Iwasaki, *Acta Crystallogr. Sect. B* **1979**, *35*, 1480–1482.

[36] A. Domenicano, L. Torelli, A. Vaciago, L. Zambonelli, *J. Chem. Soc. A* **1968**, 1351–1361.

[37] F. Jian, Z. Wang, Z. Bai, X. You, H.-K. Fun, K. Chinnakali, *J. Chem. Crystallogr.* **1999**, *29*, 227–231.

[38] D. A. Ileperuma, R. D. Feltham, *Inorg. Chem.* **1975**, *14*, 3042–3045.

[39] M. Ciampolini, C. Mengozzi, P. Orioli, *J. Chem. Soc. Dalton Trans.* **1975**, 2051–2054.

[40] P. C. Healy, A. H. White, *J. Chem. Soc. Dalton Trans.* **1973**, 284–287.

[41] H. Iwasaki, *Acta Crystallogr. Sect. B* **1973**, *29*, 2115–2124.

[42] C. S. Lai, E. R. T. Tiekink, *Z. Kristallogr. New Crystal Structures* **2002**, *217*, 593–597.

[43] F. Jian, Z. Wang, Z. Bai, X. You, H.-K. Fun, K. Chinnakali, I. A. Razak, *Polyhedron* **1999**, *18*, 3401–3406.

[44] S. C. Ngo, K. K. Banger, M. J. DelaRosa, P. J. Toscano, J. T. Welch, *Polyhedron* **2003**, *22*, 1575–1583.

[45] H.-B. Bürgi, E. Blanc, D. Schwarzenbach, S. Liu, Y. Lu, M. M. Kappes, J. A. Ibers, *Angew. Chem. Int. Ed. Engl.* **1992**, *31*, 640–643.

[46] A. Decken, R. A. Gossage, M. Y. Chan, C. S. Lai, E. R. T. Tiekink, *Appl. Organomet. Chem.* **2004**, *18*, 101–102.

[47] R. Hesse, *Ark. Kemi* **1963**, *20*, 481–484.

[48] D. D. Heinrich, J.-C. Wang, J. P. Fackler Junior, *Acta Crystallogr. Sect. C* **1990**, *46*, 1444–1447.

[49] H. Yamaguchi, A. Kido, T. Uechi, K. Yasukouchi, *Bull. Chem. Soc. Jpn.* **1976**, *49*, 1271–1276.

[50] R. Hesse, L. Nilson, *Acta Chem. Scand.* **1969**, *23*, 825–828.

[51] M. D. Pace, T. C. Christidis, J. J. Yin, J. Milliken, *J. Phys. Chem.* **1992**, *96*, 6855–6858.

[52] R. D. Dowsing, B. Nieuwenhuijse, J. Reedijk, *Inorg. Chim. Acta* **1971**, *5*, 301–308.

[53] S. V. Khangulov, A. J. Dessiki, V. V. Barynin, D. E. Ass, G. C. Dismukes, *Biochemistry* **1995**, *34*, 2015–2025.

[54] I. Romero, M.-N. Collomb, A. Deronyier, A. Llobet, E. Perret, J. Pèkaut, L. Le Pare, J.-M. Latour, *Eur. J. Inorg. Chem.* **2001**, 69–72.

[55] A. Pénicaud, A. P. Pérez-Benítez, R. Escudero, C. Coulon, *Solid State Commun.* **1995**, *96*, 147–150.

[56] K. Nagai, T. Iyoda, K. Hashimoto, A. Fujishima, *Perspectives in Organic-Inorganic Hybrid Solids*, Abstr. Int. Conf., Nagoya, Japan, **1996**, p. 118.

[57] E. I. Yudanova, D. V. Konarev, L. L. Gumanov, R. N. Lyubovskaya, *Russ. Chem. Bull.* **1999**, *48*, 718–721.

[58] M. S. Dresselhaus, G. Dresselhaus, P. C. Eklund, *Science of Fullerenes and Carbon Nanotubes*, Academic Press, San Diego, **1996**.

[59] S. Kazaoui, N. Minami, Y. Tanabe, H. J. Byrne, A. Eilmes, P. Petelenz, *Phys. Rev. B* **1998**, *58*, 7689–7700.

[60] D. V. Konarev, N. V. Drichko, R. N. Lyubovskaya, Y. M. Shul'ga, A. L. Litvinov, V. N. Semkin, Y. A. Dubitsky, A. Zaopo, *J. Mol. Struct.* **2000**, *526*, 25–29.

[61] V. Ern, R. E. Merrifield, *Phys. Rev. Lett.* **1968**, *21*, 609–611.

[62] D. V. Konarev, S. S. Khasanov, G. Saito, D. V. Lopatin, V. V. Rodaev, A. V. Umrikhin, A. L. Litvinov, R. N. Lyubovskaya, *J. Phys. Chem. Solids* **2005**, *66*, 711–715.

[63] N. S. Sariciftci, A. J. Heeger in *Handbook of Organic Conductive Molecules and Polymers* (Ed.: H. S. Nalwa), Wiley & Sons Ltd., **1997**, vol. 1, p. 414.

[64] Y. A. Ossipyan, Y. I. Golovin, D. V. Lopatin, R. B. Morgunov, R. K. Nikolaev, S. Z. Shmurak, *Phys. Stat. Sol. B* **2001**, *223*, R14–R15.

[65] A. L. Buchachenko, E. L. Frankevich, *Chemical Generation and Reception of Radio- and Microwaves*, Wiley, New York, **1994**, p. 180.

[66] *SMART and SAINT*, Area detector control and integration software, Ver. 6.01. Bruker Analytical X-ray Systems, Madison, Wisconsin, U. S.A, **1999**.

[67] G. W. Sheldrick, *SHELXTL*, An Integrated System for Solving, Refining and Displaying Crystal Structures from Diffraction Data, Version 5.10, Bruker Analytical Systems, Madison, **1997**.